JAAS

Accepted Manuscript

This is an *Accepted Manuscript*, which has been through the Royal Society of Chemistry peer review process and has been accepted for publication.

Accepted Manuscripts are published online shortly after acceptance, before technical editing, formatting and proof reading. Using this free service, authors can make their results available to the community, in citable form, before we publish the edited article. We will replace this *Accepted Manuscript* with the edited and formatted *Advance Article* as soon as it is available.

You can find more information about *Accepted Manuscripts* in the Information for Authors.

Please note that technical editing may introduce minor changes to the text and/or graphics, which may alter content. The journal's standard Terms & Conditions and the Ethical guidelines still apply. In no event shall the Royal Society of Chemistry be held responsible for any errors or omissions in this *Accepted Manuscript* or any consequences arising from the use of any information it contains.

ROYAL SOCIETY OF CHEMISTRY

www.rsc.org/jaas

Capability of fs-LA-ICP-MS for sulfide analysis in comparison to ns-LA-ICP-MS: Reduction of laser induced matrix effects?

Cora C. Wohlgemuth-Ueberwasser[1]* and Klaus Peter Jochum[2]

[1]* Department of Geological Sciences, Stockholm University, 106 91 Stockholm, Sweden. Tel: (46) 8 674 7848. E-mail: cora.wohlgemuth-ueberwasser@geo.su.se

[2] Biogeochemistry and Climate Geochemistry Departments, Max Planck Institute for Chemistry, P.O. Box 3060, D-55020 Mainz, Germany

Keywords

sulfide, LA-ICP-MS, femtosecond, melting, fractionation, PGE

Abstract

We applied three different LA systems (213 nm nanosecond solid state, 193 nm nanosecond excimer, and 200 nm femtosecond laser) coupled to a quadrupole ICP-MS or a sector field ICP-MS, respectively, to the analysis of different sulfide minerals (pyrrhotite, chalcopyrite, and sphalerite). Ablation craters were investigated via back-scattered electron (BSE) images to compare the amount of melt produced, and fractionation factors were calculated to determine the degree of down-hole fractionation. Our results show significant differences in melting between the three LA systems . While samples show massive melting when using the ns systems, no melting has been observed utilizing the fs laser. Fractionation factors for a variety of elemental pairs indicate the absence of down-hole fractionation even at highest melt production. The extend of melting of different sulfide specimen is independent of melting temperatures of these materials. Although no down-hole fractionation has been observed, Fe/S fractionation as calculated from sensitivities deviate among pyrrhotite and chalcopyrite when applying the 193 nm ns and the 200 nm fs systems. Analyses of synthetic pyrrhotite with known PGE concentrations using the 200 nm fs LA system yielded moderately precise and accurate concentration data (3-4%; 4-14% 2SD) utilizing sulfide as external reference material. Application of NIST610 as reference material improved the precision to 1.4-2.4% 2SD and the deviation from reference values to 5-7%.

Introduction

LA-ICP-MS is a nowadays widely available tool for routine *in-situ* analyses of a plethora of trace elements and isotope ratios in various matrices, not only limited to geological samples[1, 2, 3] . Developments

in the recent years include improvement of mass spectrometers with higher sensitivity as well as LA systems with shorter wave and pulse widths (cf. Ohata et al, 2014[4]). One of the major advantages of shorter wave and laser pulse widths are decreases in laser induced matrix effects that are often associated with heating or even melting of a sample under the laser beam[5]. For conventional accurate and precise determination of trace elements in geological samples by LA-ICP-MS, the ablation behaviour of the sample and the reference material applied should be as similar as possible to minimize fractionation-related inaccuracies.

Many studies described and tried to quantify chemical fractionation occurring during aerosol transport due to preferential redeposition and partial digestion in the plasma[6, 7, 8, 9]. To further investigate these effects is not the aim of this study. Additional fractionation might occur during the ablation process due to heating or even melting of a sample under the laser beam[10, 11, 12]. The process of ablation itself is widely discussed in the literature on LA fundamentals and includes phase explosion, spinodal decomposition and condensation of supersaturated vapour into particles[13, 14, 6].

Laser ablation (LA) systems with a variety of wavelengths have been applied in geosciences from 694 nm and 1064 nm in the earliest applications (cf. H. Longerich, 2008[16]. These wavelengths are useful for some bulk analyses while some minerals are poorly ablated, resulting in "catastrophic" ablation[17]. The today more common 213 nm ns Nd:YAG and 193 nm ns excimer lasers are more versatile due to their better absorption in most matrices. Both these systems operate at typical pulse widths of 4 to 5 ns[18]. Guillong et al. (2003)[19] observed increasing particle size production with increasing wavelength for 193, 213, and 266 nm ns solid state LA. Production of large particles affect elemental fractionation as the aerosol composition does not stoichiometrically represent the sample composition. Large particles also affect fractionation by incomplete decomposition and ionization in the ICP. In contrast to the pulse duration of ns lasers, fs lasers operate at <0.00015 ns, minimizing elemental fractionation due to shorter interaction with the sample, less thermal effects, and production of ultra-fine aerosol particles[20].

Few studies tried to quantify fractionation effects of sulfides applying femtosecond laser ablation. From earlier studies utilising nanosecond laser systems a strong melting of sulfides has been reported, leading to evaporation of S and possible fractionation of chalcophile and siderophile elements between the ablated sulfide and the produced sulfide melt. Melting of the sample under the laser beam requires matrix matched reference materials that experience the same degree of melting.

A variety of studies in over two decades investigated fractionation effects utilizing fs LA systems. Russo et al. (2002)[10] observed no elemental fractionation for most elements in NIST 610 using an 800 nm fs laser. Poitrasson et al. (2003)[21] compared ns and fs LA of glass, monazite, and zircon and observed much less elemental fractionation for Pb/U applying the fs system. They also investigated the resulting ablation craters and observed more obvious melting effects in ablation craters in NIST 610 produced by the ns laser compared to the fs system. Horn and von Blanckenburg (2007)[22] investigated elemental and isotopic fractionation during fs LA of a variety of geological materials, including Fe-isotope fractionation in Fe-sulfide. They report the absence of isotopic Pb/U and Th/U fractionation as well as elemental fractionation even with the application of non-matrix matched reference materials for calibration. Garcia et al. (2007)[11] studied elemental fractionation by fs LA of multi-component glasses as well as binary metallic and semiconductor samples. They observed strong interelement fractionation only during the first shots of the laser, but stoichiometric element ratios after this initial ablation phase. Glaus et al. (2010)[23] and Diwakar et al. (2013)[24] observed reduced fractionation of Cu and Zn from fs LA of brass compared to ns LA.

Glaus et al. (2010)[23] compared the ablation behaviour of pyrite and galena by ns and fs LA and found no fractionation of S relative to Fe for both systems. This is in contrast to observations by Gilbert et al. (2014)[5] who reported significant fractionation of S relative to Fe applying ns LA and found a correlation between the extent of melting of the sample and S fractionation. They accounted this to the higher volatility of S relative to Fe, which has also been reported by Horn and von Blanckenburg (2007)[22] for ns LA. For fs LA, Horn and von Blanckenburg (2007)[22] reported no fractionation of volatile elements. Velásquez et al. (2012)[25] observed no differences in Au and Cu concentration in pyrite using sulfide and NIST 610 as reference material applying fs LA. D'Abzac et al. (2013)[26] analyzed Fe isotopes in oxides, carbonates and sulfides, namely pyrrhotite and pyrite. They attributed any elemental and isotopic fractionation to particle generation processes and not laser – matter interaction. They also reported elemental Fe/S fractionation to be different for different sulfide minerals. Vanhaecke et al. (2010)[27] analyzed PbS fire assay buttons for PGE and Au by fs LA and reported improved measurement accuracy with the use of fs LA compared to ns LA.

Overall, the literature is divided as to if and how elemental and isotopic fractionation occurs during fs LA. For sulfides, limited data are available and no systematic study on the comparison of ns and fs LA on fractionation, measurement accuracy and precision applied to different sulfide minerals has been conducted so far.

Methods

Within this study, three sulfide samples were analyzed: synthetic pyrrhotite (po) $Fe_{1-x}S$[28], natural chalcopyrite (ccp; $CuFeS_2$) (sample 58-7H) and natural sphalerite (sp; ZnS) (sample 69RD(8-12)) (~5 %m/m Fe) from hydrothermal black smoker samples[29] .These minerals were selected for their different melting temperatures and for being among the most common sulfide minerals in ore deposits.

A synthetic Ni-sulfide (NiS3[30]) was used as one of the reference materials and was included in investigations of melting effects on the ablation site. While po has a melting temperature of ~1050°C at this composition (39 %m/m S[31]), NiS already melts at ~800°C[32, 33] and ccp at even lower temperatures of ~550°C[34, 35]. In contrast, sp is reported to start sublimating at 1185°C instead of melting[36]. Vanhaecke et al. (2010)[27] have shown that melting might occur even applying fs LA for PbS fire assay buttons with a melting temperature of ~330°C.

The sulfide grains were embedded in epoxy resin and polished prior to analysis. Three different laser systems have been utilized: UP 213 nm ns Nd:YAG (PetroTectonics Facility, Stockholm University), 193 nm ns excimer (PetroTectonics Facility, Stockholm University) and NWR Femto200 femtosecond laser (Biogeochemistry Department, Max Planck Institute for Chemistry, Mainz). Besides the different wavelength a major difference between the laser systems are pulse widths of 4 and 5 ns for the 213 nm and the 193 nm ns LA, respectively, and <0.00015 ns for the 200 nm fs LA[18]. The 213 nm and 193 nm ns LA systems were coupled to a Thermo XSeries 2 quadrupole ICP-MS while the 200 nm fs LA was operated with a Thermo Element 2 sector field ICP-MS.

Melt production during ablation of sulfides has already been reported by Wohlgemuth-Ueberwasser et al. (2007)[28], who showed a strong dependency on laser energy density. To verify melt production during ablation, 20 shots applying a 75 µm spot size with 3 and 7 J cm^{-2} with both systems the 213 and 193 nm ns LA have been produced. Previous studies have shown that energy densities between 3 and 7 J cm-2 are suitable for sulfide analyses (Wohlgemuth-Ueberwasser 2007[28]). Femtosecond LA requires much lower energy densities and significantly less material is ablated. Therefore, we applied energy densities of 0.14 and 0.25 J cm^{-2} and 100 single shots to investigate ablation craters for melt production. The use of a low energy density supresses the formation of large particles that cannot be sufficiently ionized in the ICP[37].The ablation craters were subsequently imaged using a Quanta FEG 650 ESEM with low vacuum, 20 kV and a CBS detector at the PetroTectonics Facility, Stockholm University.

For all three sulfide minerals and laser types quantitative ICP-MS analyses were conducted including the analysis of S, Fe, Ni, Cu, and Zn to verify any fractionation during ablation. Pyrrhotite was additionally quantified for Rh, Pd, and Pt with 10 analyses each for the three LA systems. Each spot analysis consisted of 30 s background (gas blank), 60 s ablation and 60 s wash-out applying a 50, 55 or 60 µm spot size depending on the apertures of the different LA systems. Instrumental and analytical details are given in table 1. Applying the 200 nm fs LA system, external standardization on NIST 610 was carried out with line analyses due to a strong intensity decrease with increasing crater depth[18] due to poor sample-beam interaction (Supplement 1). ^{108}Pd was used for NiS3 analyses to account for any possible contribution from ^{65}Cu^{40}O on the signal although Cu concentrations are negligible while ^{105}Pd was used for NIST 610 to avoid the ^{108}Cd interference.

	NWR-UP-213	**NWR-193**	**NWR Femto200**
Laser ablation:			
laser type	NWR New Wave UP 213 Nd:YAG laser	ESI New Wave ArF 193 nm excimer laser	NWR Femto200 femtosecond laser
laser energy density	3 and 7 J cm^{-2}	3 and 7 J cm-2	0.14 and 0.25 J cm^{-2}
laser frequency	8 Hz	8 Hz	50 Hz
beam diameter	50 and 75 µm	60 and 75 µm	55 µm
ICP-MS:			
ICP-MS instrument	Thermo XSeries2	Thermo XSeries2	Thermo Element 2
plasma power [W]	1400	1400	1060
sample gas [ml/min]	500 He	500 He	0.6 Ar, 0.7 He
auxiliary gas [l/min]	0.72 Ar	0.72 Ar	1 Ar
cooling gas [l/min]	13 Ar	13 Ar	16 Ar
nebulizer gas [l/min]	0.94 Ar	0.94 Ar	-
acquisition mode	pulse counting	pulse counting	analogue and pulse counting
dwell times [ms]	^{33}S (10), ^{56}Fe (10), ^{60}Ni (10), ^{65}Cu (10), ^{66}Zn (10), ^{103}Rh (30), ^{105}Pd (30), ^{108}Pd (30), ^{195}Pt (30), ^{196}Pt (30)	^{33}S (10), ^{56}Fe (10), ^{60}Ni (10), ^{65}Cu (10), ^{66}Zn (10), ^{103}Rh (30), ^{105}Pd (30), ^{108}Pd (30), ^{195}Pt (30), ^{196}Pt (30)	^{33}S (30), ^{34}S (30), ^{57}Fe (30), ^{62}Ni (30), ^{65}Cu (30), ^{66}Zn (30), ^{67}Zn (30), ^{68}Zn (30), ^{103}Rh (30), ^{105}Pd (30), ^{108}Pd (30), ^{195}Pt (30), ^{196}Pt (30)

Table 1: Instrumental parameters and analytical conditions of the LA-ICP-MS systems applied for quantitative analyses.

Data reduction was performed off-line through the software Iolite[38, 39], using the Trace_Elements_IS data reduction scheme[40]. For analyses applying NIST610 as reference material, Fe was used as internal standard (IS), while for NiS3 as reference material, S or Ni were used as IS. The corresponding data is referred to as NiS3(S) and NiS3(Ni).

Fractionation factors have been calculated for different elements following the method of Fryer et al. (1995)[41] by dividing the background subtracted counts per second of the second half of an ablation spectrum by those of the first half. Background cps are between 0.01 and 3% of the cps during ablation. If

no fractionation occurs the F.F. should be at unity. A 2-sigma outlier rejection has been applied to eliminate strong spikes, especially for Fe in NiS3, which shows a variation of 15-20% (3 to 6 data points rejected).

Results

Quantitative results

Quantitative concentrations of Rh, Pd, and Pt in po reveal differences between the three LA systems applied as well as between the different internal standards and reference materials used (table 2; figure 1). The accuracy is expressed as percentage measurement errors. Precision or deviation from reference values (in percent) is calculated to evaluate the difference between measured and reported concentrations. Measurements of Rh concentrations with 213 nm ns LA give low measurement errors (<3.8%) and moderately precise (<9.4% 2SD) values using NiS3 as reference material and S or Ni as internal standard. In contrast external calibration with NIST 610 show very precise (4.0% 2SD) but inaccurate (>14.5%) results for Rh concentrations (figure 1 A). The latter is also true for Rh concentrations applying 193 nm ns LA, with high precision (4.4% 2SD) and high deviation from reference values (17%) using NIST 610. The high deviation from reference values might partly be attributed to poorly defined reference values for these elements in NIST 610. The use of NiS3 as reference material and S as internal standard provide lower precision (9.1% 2SD) but less deviation from reference values (<5.4%) while values for Rh concentrations with the use of Ni as internal standard are outside the uncertainty range of the published values for po, with a precision of 4.5% and a deviation from reference values of >24%. Analyzing Rh concentrations in po with 200 nm fs LA provides accurate and precise values independent of the external or internal standard applied. Deviation from reference values of 4.2 – 6.1% could be achieved with a precision of 3.0 – 3.5% 2SD with NiS3 as reference material and 1.1% with NIST 610 as reference material.

	laser	true value	2 SD	**NiS3(S)**	2SD	2SD%	*d. r. v. (%)*	**NiS3(Ni)**	2SD	2SD%	*d. r. v. (%)*	**NIST 610**	2SD	2SD%	*d. r. v. (%*
Rh	213 nm ns	57,20	7,00	**56,36**	4,85	8,60	*1,46*	**55,03**	5,18	9,41	*3,79*	**48,79**	1,93	3,95	*14,70*
Pd	213 nm ns	60,40	2,80	**81,47**	3,41	4,19	*-34,88*	**70,38**	6,69	9,51	*-16,52*	**68,54**	9,33	13,61	*-13,48*
Pt	213 nm ns	60,20	1,90	**62,38**	3,07	4,93	*-3,62*	**58,02**	5,29	9,12	*3,62*	**53,59**	3,32	6,19	*10,98*
Rh	193 nm ns	57,20	7,00	**60,28**	5,17	8,58	*-5,38*	**71,01**	3,22	4,54	*-24,14*	**47,71**	2,10	4,41	*16,59*
Pd	193 nm ns	60,40	2,80	**66,24**	4,08	6,15	*-9,67*	**66,50**	4,06	6,10	*-10,10*	**55,80**	4,38	7,85	*7,62*
Pt	193 nm ns	60,20	1,90	**60,27**	3,02	5,02	*-0,12*	**71,85**	4,88	6,79	*-19,35*	**47,67**	4,00	8,40	*20,81*
Rh	200 nm fs	57,20	7,00	**60,68**	2,14	3,52	*-6,08*	**59,62**	1,81	3,04	*-4,24*	**60,75**	0,66	1,09	*-6,21*
Pd	200 nm fs	60,40	2,80	**68,52**	3,36	4,90	*-13,44*	**68,10**	1,92	2,82	*-12,75*	**44,83**	0,72	1,62	*25,77*
Pt	200 nm fs	60,20	1,90	**55,79**	3,72	6,66	*7,33*	**56,44**	1,96	3,48	*6,25*	**61,82**	1,28	2,07	*-2,69*

Table 2: Concentration of Rh, Pd, and Pt in po obtained with the three different LA systems and the different reference materials and internal standards applied. Note that for NIST610 ^{105}Pd was used while for NiS3 ^{108}Pd. d. r. v. = deviation from reference values. n=10 for all analyses.

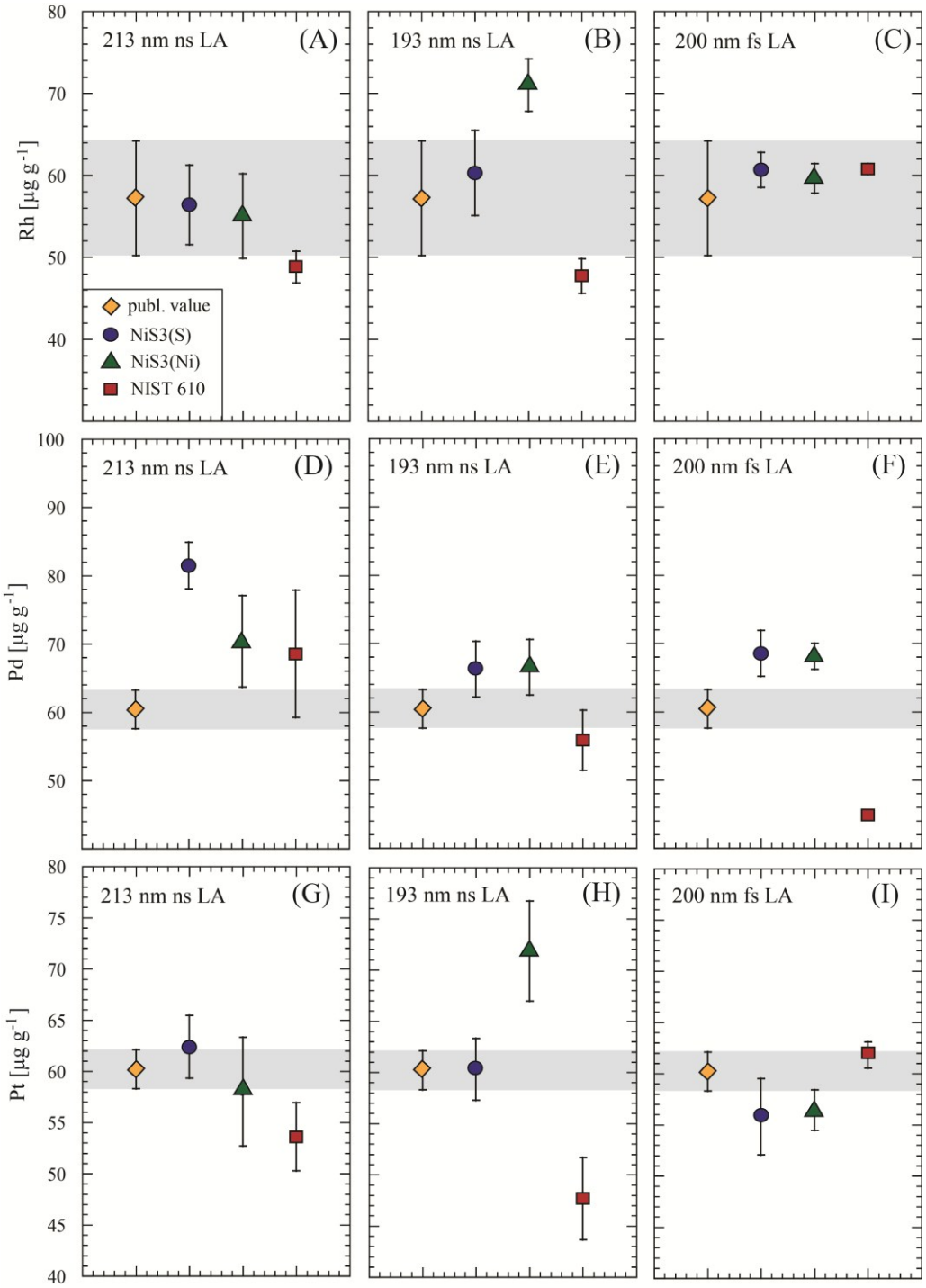

Figure 1: Concentrations of Rh, Pd, and Pt in po derived from the three different LA systems with application of NiS3 and NIST 610 as reference materials and S and Ni as internal standards for NiS3.

The values obtained for Pd concentrations in po are more variable with most analytical setups not providing accurate numbers. Analyses with 213 nm ns LA yield deviations from reference values of 13.5 – 35% while precision varies from 4.2 – 13.6% 2SD. Only analyses applying NIST 610 as reference material produce results that meet the published values within uncertainty. Results of 193 nm ns LA are matching the published values within uncertainty with all three standardization settings with deviations from

reference values from 7.6 – 10.1% and a precision of 6.1 – 7.9% 2SD. Application of 200 nm fs LA produced too high values with the use of NiS3 and too low values with the use of NIST 610 as reference materials.

The application of 213 nm ns LA for the analysis of Pt concentrations in po provides accurate (3.6%) and moderately precise (4.9 and 9.1%) analyses using NiS3 as reference material. The values for Pt concentrations with Ni as internal standard are in this case less precise than with the use of S as internal standard. The use of NIST 610 produced precise (6.2%) but inaccurate values (11%) that do not meet published values within uncertainty limits. With 193 nm ns LA, precision is high and deviation from reference values is low with NiS3(S) (5% and 0.1% respectively), while values obtained with NiS3(Ni) and NIST 610 are far off the published values (table 2; figure 1 H). In contrast, 200 nm fs LA produced moderately accurate (2.7 – 7.3%) values with a precision of 2.1 – 6.7% 2SD with all three LA setups.

Melting and fractionation

Investigation of the ablation craters by SEM revealed the strongest melting with application of the 213 nm ns LA and less melting with the 193 nm ns LA. With 200 nm fs LA no melt could be observed around or inside the ablation craters. There are also strong differences in melting of the different sulfide specimens ablated with the highest melt production in NiS3 (figure 2), followed by po (figure 3) and ccp (figure 4) and least melting in sp (figure 5). The amount of melt correlates with the laser energy density applied, but not with the melting temperatures of the different sulfide specimen. The craters produced by 200 nm fs LA differ significantly from ns ablation craters and between the different sulfides. Ablation of po and ccp produced filament like structures that might be similar to those described by Russo et al. (2002)[10] for glass ablation and which they attributed to non-linear self-focusing during the fs laser pulse. Ablation craters in sp are more comparable to those produced by ns LA with less rounded ablation pits but more sufficient penetration into the sample. NiS3 shows less controlled ablation with frayed crater rims and uneven structures within the ablation craters.

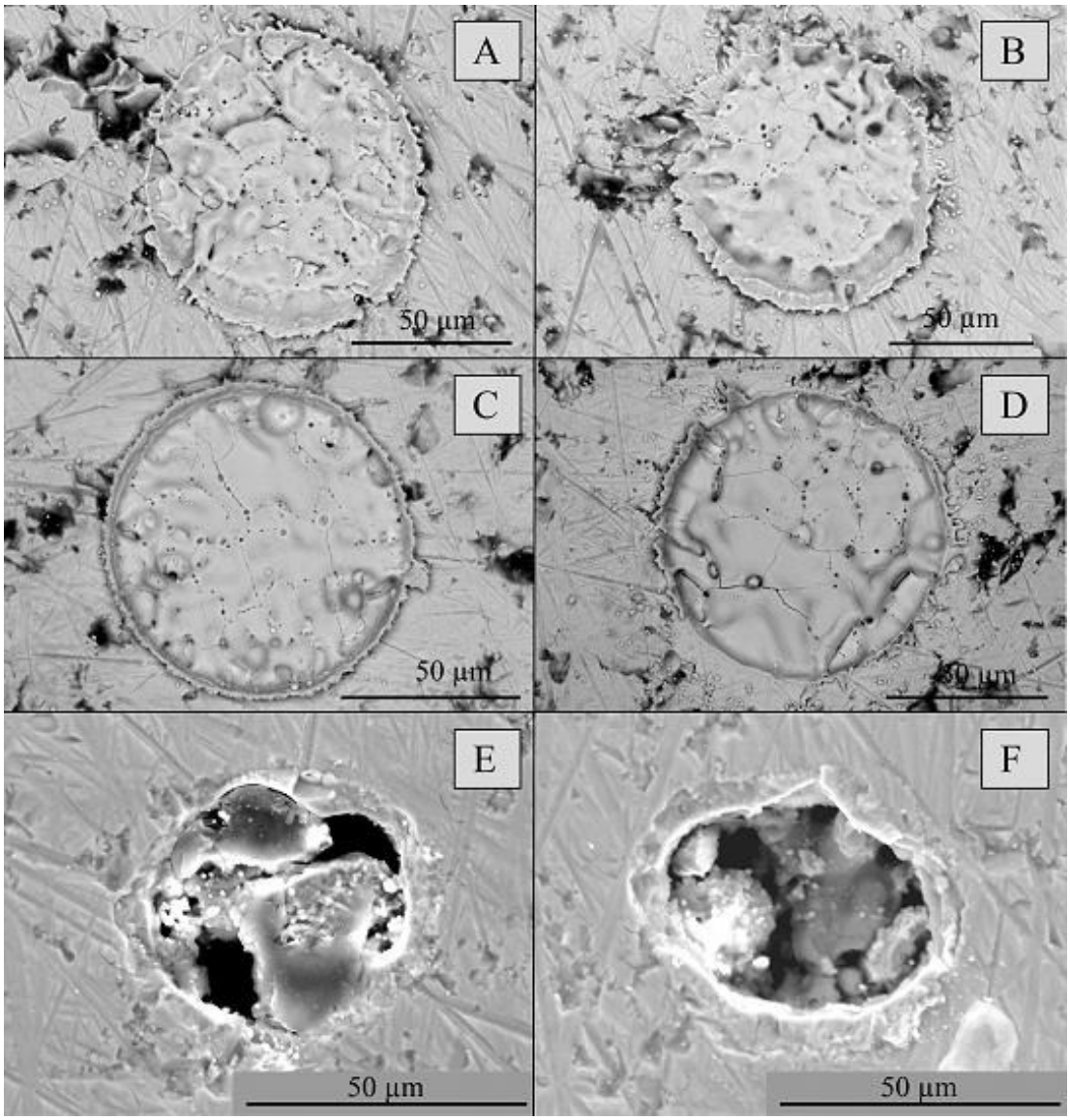

Figure 2: BSE images of ablation craters in NiS3 produced with (A) 213 nm ns LA and 3 J cm^{-2}; (B) 213 nm ns LA and 7 J cm^{-2}; (C) 193 nm ns LA and 3 J cm^{-2}; (D) 193 nm ns LA and 7 J cm^{-2}; (E) 200 nm fs LA and 0.14 J cm^{-2}; (F) fs LA and 0.26 J cm^{-2}.

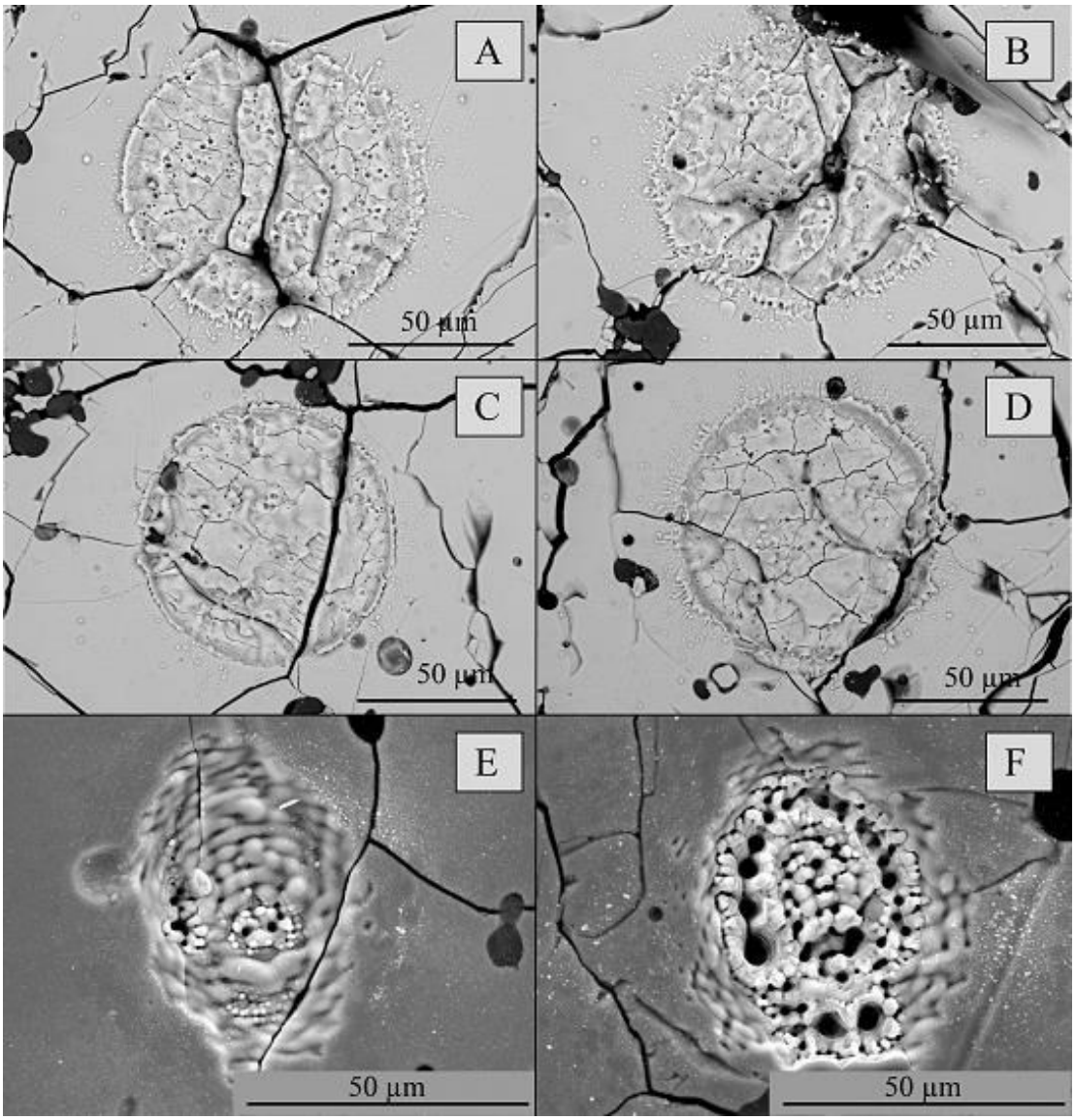

Figure 3: BSE images of ablation craters in po produced with (A) 213 nm ns LA and 3 J cm^{-2}; (B) 213 nm ns LA and 7 J cm^{-2}; (C) 193 nm ns LA and 3 J cm^{-2}; (D) 193 nm ns LA and 7 J cm^{-2}; (E) 200 nm fs LA and 0.14 J cm^{-2}; (F) fs LA and 0.26 J cm^{-2}.

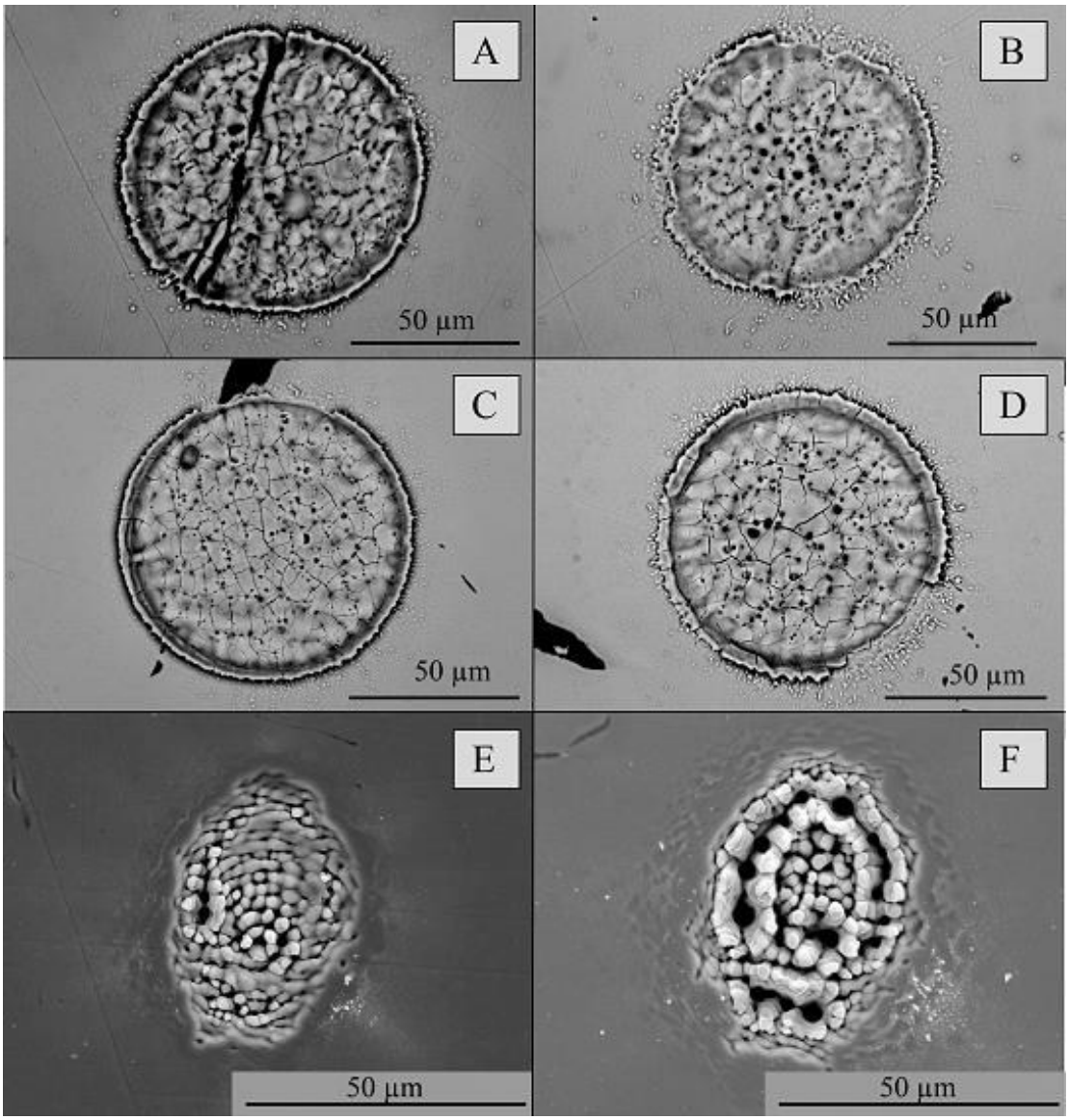

Figure 4: BSE images of ablation craters in ccp produced with (A) 213 nm ns LA and 3 J cm^{-2}; (B) 213 nm ns LA and 7 J cm^{-2}; (C) 193 nm ns LA and 3 J cm^{-2}; (D) 193 nm ns LA and 7 J cm^{-2}; (E) 200 nm fs LA and 0.14 J cm^{-2}; (F) fs LA and 0.26 J cm^{-2}.

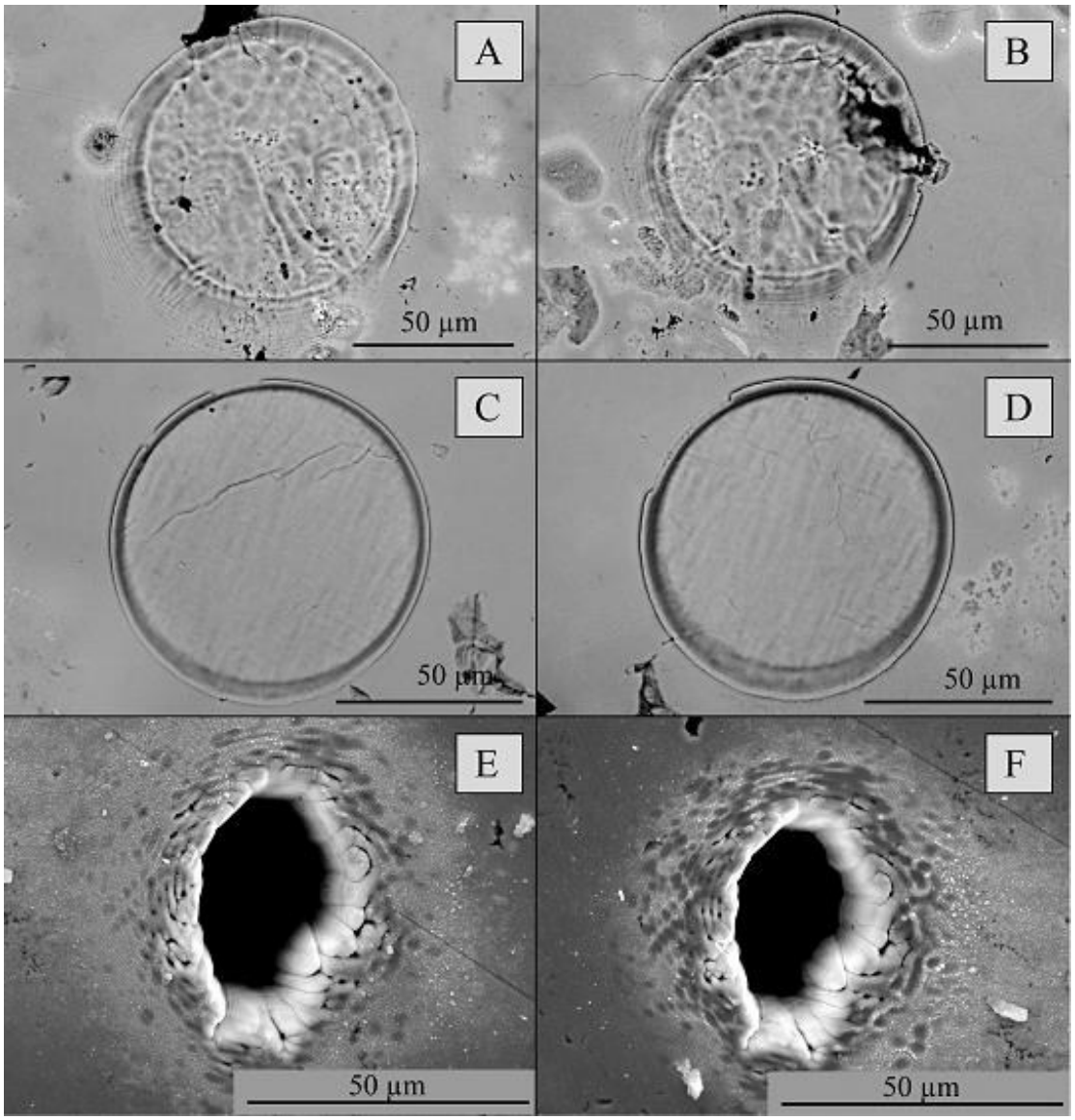

Figure 5: BSE images of ablation craters in sp produced with (A) 213 nm ns LA and 3 J cm^{-2}; (B) 213 nm ns LA and 7 J cm^{-2}; (C) 193 nm ns LA and 3 J cm^{-2}; (D) 193 nm ns LA and 7 J cm^{-2}; (E) 200 nm fs LA and 0.14 J cm^{-2}; (F) fs LA and 0.26 J cm^{-2}.

Calculated fractionation factors (F.F.) show strongest deviation from 1 (highest fractionation) for NiS3 with application of 193 nm ns LA. F.F. are closer to unity with 213 nm ns LA and 200 nm fs LA. Elemental pairs that are significantly affected by fractionation are those including the PGE independent of the combination with Fe, Ni, or S (Figure 6). Although no melting could be observed for 200 nm fs LA, F.F. are generally not closer to unity than with ns LA.

NiS3	FF 213 nm ns	2SD	FF 193 nm ns	2SD	FF 200 nm fs	2SD
Rh/Fe	1,21	0,44	1,41	0,29	0,92	0,15
Pt/Fe	1,22	0,44	1,49	0,22	0,94	0,13
Pd/Fe	1,22	0,53	1,38	0,27	0,88	0,18
Rh/S	0,98	0,14	1,22	0,34	1,07	0,12
Pt/S	0,99	0,19	1,31	0,39	1,10	0,12
Pd/S	0,98	0,09	1,16	0,11	1,03	0,10
Rh/Ni	1,00	0,16	1,18	0,29	1,09	0,10
Pt/Ni	1,01	0,21	1,27	0,35	1,12	0,11
Pd/Ni	1,00	0,08	1,12	0,10	1,05	0,09
Ni/S	0,99	0,04	1,03	0,03	0,98	0,04
Fe/S	0,84	0,24	0,88	0,18	1,18	0,23
Ni/Fe	1,23	0,53	1,24	0,28	0,84	0,18
ccp	FF 213 nm ns	2SD	FF 193 nm ns	2SD	FF 200 nm fs	2SD
Cu/S	0,95	0,03	0,89	0,05	1,01	0,03
Cu/Fe	1,01	0,04	0,97	0,02	0,99	0,01
Zn/Cu	1,08	0,15	1,12	0,28	1,00	0,17
Zn/Fe	1,09	0,17	1,10	0,27	0,98	0,16
sp	FF 213 nm ns	2SD	FF 193 nm ns	2SD	FF 200 nm fs	2SD
Zn/Fe	1,05	0,22	0,96	0,14	0,84	0,29
Zn/S	0,98	0,03	0,97	0,04	0,88	0,26
Fe/S	0,94	0,18	1,02	0,13	1,05	0,40
po	FF 213 nm ns	2SD	FF 193 nm ns	2SD	FF 200 nm fs	2SD
Rh/Fe	1,08	0,04	1,08	0,07	1,05	0,04
Pt/Fe	1,05	0,07	1,08	0,14	1,07	0,06
Pd/Fe	1,04	0,05	1,04	0,12	1,07	0,07
Rh/S	1,02	0,10	1,03	0,10	0,96	0,07
Pt/S	0,99	0,13	1,03	0,14	0,97	0,06
Pd/S	0,99	0,10	0,99	0,11	0,98	0,04
Rh/Ni	1,09	0,08	1,12	0,15	1,00	0,33
Pt/Ni	1,06	0,08	1,13	0,20	1,02	0,36
Pd/Ni	1,05	0,07	1,09	0,20	1,03	0,33
Fe/S	0,94	0,07	0,95	0,08	0,91	0,07
Ni/S	0,95	0,08	0,81	0,52	0,99	0,13
Fe/Ni	1,00	0,07	1,04	0,16	0,96	0,32
NIST	FF 213 nm ns	2SD	FF 193 nm ns	2SD	FF 200 nm fs*	2SD
Rh/Fe	1,08	0,16	1,05	0,05	n.a.	n.a.
Pt/Fe	1,09	0,15	1,00	0,07	n.a.	n.a.
Pd/Fe	0,97	0,19	0,98	0,06	n.a.	n.a.
Fe/Ni	0,95	0,07	0,98	0,02	n.a.	n.a.
Fe/Cu	0,92	0,12	0,97	0,02	n.a.	n.a.
Fe/Zn	0,83	0,18	0,99	0,06	n.a.	n.a.
Cu/Zn	0,90	0,11	1,02	0,04	n.a.	n.a.

Table 3: Fractionation factors calculated for available element pairs following Fryer et al. (1995). n=10 for all analyses.

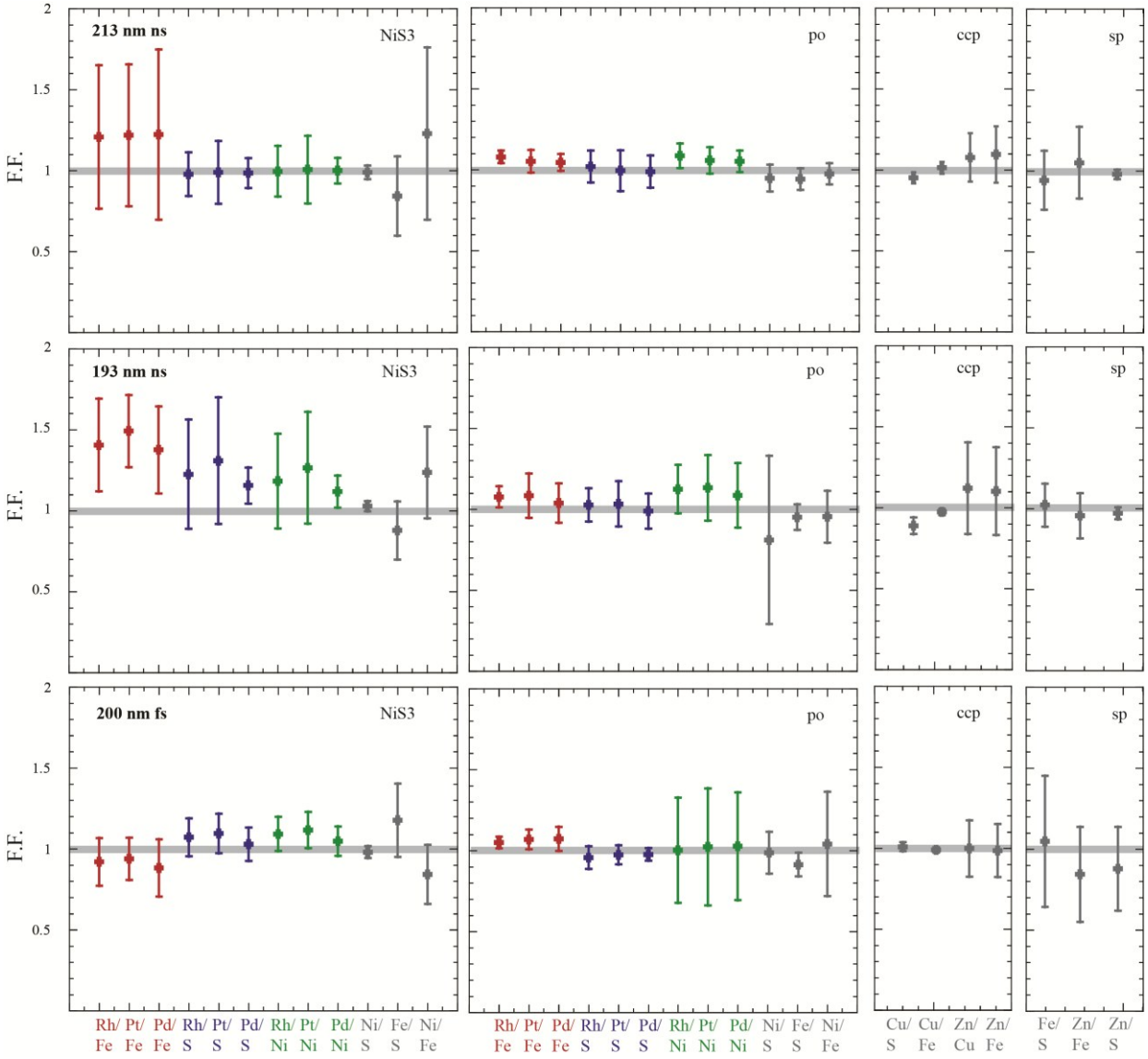

Figure 6: Fractionation factors for the different sulfide specimen analyzed with the three LA systems.

Discussion

A couple of factors need to be considered when evaluating the measurement accuracy and precision obtained by LA-ICP-MS of PGE as well as other trace elements in sulfide minerals. These include the LA system utilized, the reference material and internal standard applied and the interaction of the laser beam with the sample, which might result in elemental fractionation.

Melting and laser induced elemental fractionation

Earlier contributions assigned fractionation during sulfide LA to melting of the sample under the laser beam[15]. This is supposed to lead to the evaporation of the more volatile S relative to metals. Additionally,

a melt produced during ablation might fractionate chalcophile elements in the generated melt, depleting the aerosol in these elements. We chose three PGE of which Pt and Pd have low sulfide / sulfide melt partition coefficients (<1) and Rh with a partition coefficient >1[42]. Therefore, Pt and Pd could be depleted in the aerosol during melting as response of LA, while Rh could be enriched. Highest fractionation should be expected for those sulfide samples with the lowest melting T and ablation with the LA system that produces largest amounts of melt. In contrast to this, the absence of melting should produce F.F. around unity.

Largest amounts of melt have been produced within this study by LA of ccp and NiS (melting T of ~550°C and ~800°C, respectively) applying the 213 nm ns LA, with slightly less melting occurring with application of 193 nm ns LA (Figures 2 and 4). Fractionation factors allow for a quantitative evaluation of the influence of melting on the fractionation of trace elements relative to the applied internal standard as well as major elements to each other. The F.F. of ccp for Zn/Cu and Zn/Fe are around unity with large 2-sigma uncertainties (Figure 6). These large uncertainties can be attributed to the low Zn concentration in ccp (< 0.1 %m/m[29]). F.F. for Cu/Fe are at unity while Cu/S vary for the three different LA systems. They deviate most significantly with application of the 193 nm ns system compared to the 213 nm ns and the 200 nm fs system. If melting would be the controlling factor for the fractionation observed here, then the deviation from unity should be highest with utilization of the 213 nm ns system. No melting has been observed with use of 200 nm fs LA and F.F. in ccp are at 1 for all elemental pairs.

NiS3 experienced approximately the same degree of melting under the two ns LA systems, and no melting with the fs LA (Figure 2). According to this, F.F for fs LA are at 1 within uncertainty. Although melting is more extensive with application of the 213 nm ns system compared to 193 nm ns system, F.F. deviate stronger from unity with 193 nm ns LA. PGE/Fe (Rh/Fe, Pt/Fe, and Pd/Fe) show strong fractionation with F.F. of 1.38 to 1.49 (Table 3). This can be related to the low Fe concentration in NiS3 with 350 µg g^{-1} [30]. The F.F. for PGE/Ni and PGE/S are close to 1 with application of the 213 nm ns and the 200 nm fs systems, while the F.F. with utilization of the 193 nm ns system results in strong fractionation. While Rh/S, Rh/Ni, Pt/S, and Pt/Ni have F.F. around unity within uncertainty, Pd/S and Pd/Ni do not. It needs to be noted that uncertainties on the PGE/S F.F. calculated for NiS3 are significantly larger than those for the same element pairs in po. This might be attributed to a more heterogeneous distribution of the PGE in NiS3 compared to po. Although F.F. reflect the fractionation between elemental pairs, its uncertainty is strongly related to the homogeneous distribution of the corresponding elements in the analysed sample. Large uncertainty for PGE F.F. in NiS3 might therefore be related to the heterogeneous distribution of the PGE within this matrix. To verify this possible heterogeneity we calculated the 2SD for the two PGE

containing matrices NiS3 and po (table 4), which shows for the 193 nm ns LA highest variation with 7.3 and 12.3% for NiS3 and 1.8 to 3.4% for po. Analyses with the two other LA systems reveal less significant heterogeneity in NiS3 but still stronger heterogeneity than in po.

This heterogeneity in trace element distribution in NiS3 can also be observed in the ablation spectra (Figure 7). Arrows 1 to 5 mark time slices of the spectra where intensity, especially for Rh and Pt, vary significantly. In contrast, spectra of po are generally flat (Figure 7 D to F) only showing spikes in intensity for Ni (arrow 6) reflecting the heterogeneous distribution of Ni in po. Variations in PGE generally correlate with variations in major elements and can be attributed to variation of aerosol produced and / or transported to the ICP-MS (arrow 7).

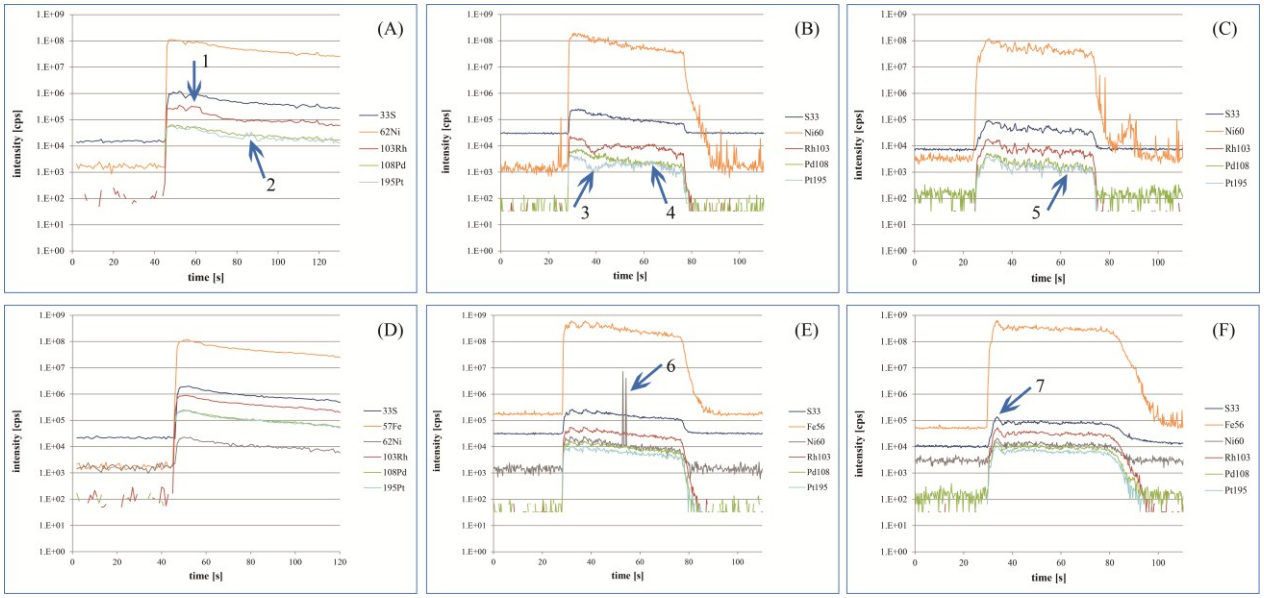

Figure 7: Ablation spectra in intensity (cps) versus time. (A): NiS3 with the 200 nm fs LA; (B): NiS3 with the 193 nm ns LA; (C): NiS3 with the 213 nm ns LA; (D): po with the 200 nm fs LA; (E): po with the 193 nm ns LA; (F): po with the 213 nm ns LA. Arrows "1" – "5" point to heterogeneities in the PGE distribution in NiS3. Arrow "6" shows the heterogeneous distribution of Ni in po. Arrow "7" points to an intensity spike at the start of ablation which is not attributed to heterogeneities as all elements are affected, but reflects differences in ablation and / or transport efficiency during ablation.

For po melting is less pronounced than for ccp and NiS, and sp is least affected which corresponds to the melting / sublimation T of 1050°C and 1185°C, respectively. Nevertheless, there seems to be minor fractionation of PGE/Fe as well as slight fractionation of PGE/Ni for the ns LA systems. PGE/S F.F. are at 1 for all three laser systems. The F.F. for Ni/S for po with the 193 nm ns system is distinctly <1 and shows

large uncertainties which can be attributed to the low Ni concentration in po of around 88 µg g^{-1} and its heterogeneous distribution with a 2 SD of >10%.

The F.F. only accounts for fractionation effects during ablation while deepening of the crater. Nevertheless, there might be fractionation between elements that occur throughout the ablation process, yielding F.F. at unity. Most F.F. calculated within this study are around 1 which does not support observations of Garcia et al. (2007)[11] who described interelement fractionation during the first shots of the laser, but stoichiometric element ratios after this initial ablation phase which then would produce F.F. that deviate from 1. Investigation of element ratios over the complete time of ablation do not show any elemental fractionation at the start of ablation for any of the three LA systems. To further investigate the relationship between melting and fractionation, we calculated Fe/S ratios for po and ccp from the background subtracted counts per second (Table 5). The Fe/S ratio is by a factor of 2 higher applying the 213 nm ns LA compared to the 193 nm ns LA system for po as well as for ccp. This means that either the response for Fe is higher or the response for S is lower with the use of 213 nm ns LA. To further evaluate this, we calculated the sensitivity for Fe and S from 213 and 193 nm ns LA and 200 nm fs LA for po and ccp (Table 5). For the 213 nm ns LA system the sensitivity is similar for S and Fe for both sulfide matrices, reflected in S po/ S ccp and Fe po/ Fe ccp ratios around 1. It should be noted that melting for these two matrices occurred to about the same extend (figures 3 and 4). S po/ S ccp and Fe po/ Fe ccp ratios from 193 nm ns LA deviate strongly from one with 0.5 and 0.6, respectively. This means that S and Fe are equally affected by a process that influences sensitivity, which in this case cannot be the volatility of S. 200 nm fs LA produces Fe po/ Fe ccp ratios close to 1 and S po/ S ccp that strongly deviate from 1 (1.8), although no melting has been observed. This fractionation of S between different mineral specimen cannot be explained yet and needs further systematic investigation. The overall difference in sensitivity of the 200 nm fs LA compared to the ns LA systems is related to the lower energy density used producing less amount of aerosol as well as to the use of a sector field MS (Element 2) with different dwell times and partly different isotopes analyzed, compared to the XSeries 2 quadrupole ICP-MS utilized with the ns LA systems.

The effect of melting on the sensitivity ratios is less pronounced with application of the 213 nm ns LA although the amount of melting is higher. This implies that melting is not responsible for different sensitivities or F.F. that strongly deviate from 1 with the 193 nm ns LA. Other factors might contribute to the quality of data produced with the 193 nm ns LA systems, which produces some low measurement accuracy data for the PGE (Figure 1), high F.F. (Figure 6) and strong differences in sensitivity between po and ccp. One reason might be a less controlled ablation or interaction between laser beam and sample.

Nevertheless this has not been observed by Wohlgemuth-Ueberwasser et al. (2007)[28] applying a 193 nm ns LA. The 193 nm ns system applied within this study is equipped with a two-volume cell with control of the movement of the ablation cup by a magnet. It needs further investigation on how this magnet might influence the behaviour of metals in the aerosol.

		Rh	2SD	2SD %	Pd	2SD	2SD %	Pt	2SD	2SD %
213 nm ns	NiS3(Ni) (n=12)	22,9	0,9	3,9	24,4	1,0	3,9	22,5	0,8	3,6
	po(Ni) (n=10)	54,9	1,4	2,6	70,3	2,3	3,3	57,5	1,8	3,1
193 nm ns	NiS3(Ni) (n=12)	22,0	1,6	7,3	24,2	1,9	7,9	22,7	2,8	12,3
	po(Ni) (n=10)	67,4	1,2	1,8	64,8	2,2	3,4	69,2	2,3	3,3
200 nm fs	NiS3(Ni) (n=12)	22,9	1,6	7,0	24,2	0,9	3,7	22,6	1,6	7,1
	po(Ni) (n=10)	59,6	2,5	4,2	68,1	2,2	3,2	56,4	2,7	4,8

Table 4: Homogeneity of PGE in NiS3 and po applying Ni as IS.

Although melting occurs with ns LA, no effect can be observed for enrichment or depletion of the PGE as would be expected from their different partition coefficients sulfide/ sulfide melt. A possible explanation might be that melt is not only observed around the crater rim but also on the bottom of the crater. During ablation solid sulfide and generated sulfide melt on the crater bottom are ablated simultaneously and different partitioning behaviour of the PGE as well as S and Fe are irrelevant.

		213 nm ns LA		193 nm ns LA		200 nm fs LA	
			2SD %		2SD %		2SD %
raw data ratio	Fe/S po	4541	5	2296	8	52	8
	Fe/S ccp	2120	9	1087	15	30	2
sensitivity [cps/wt.%]	S po	1949	19	2826	13	19829	12
	Fe po	5659611	25	4198702	20	79165	13
	S ccp	2036	4	5341	14	11114	12
	Fe ccp	5027440	14	6888333	9	75417	12
sensitivity ratios	S po/ S ccp	0,96		0,53		1,78	
	Fe po/ Fe ccp	1,13		0,61		1,11	

Table 5: Fe/S ratios and sensitivities for Fe and S for the different LA systems.

Choice of the internal standard

The internal standard applied for LA-ICP-MS must fulfil some important criteria. First, the element should be abundant enough to be analyzed at high measurement accuracy and precision within the reference material applied as well as in the sample analyzed. Secondly, it needs to be homogeneously distributed in reference material as well as in the sample, as during data processing (e.g. with Iolite) the heterogeneity of the internal standard is not accounted for. Third, it should have approximately similar concentrations in the reference material and the sample as strong differences in concentration between

reference material and sample might affect the measurement accuracy of analyses. Additionally it should have similar volatility and first ionization potential as the analyte as well as the same extent of fractionation.

For sulfides usually major elements are used as internal standard, which may be Zn[43], Fe[44,25], S[45], or Ni[30]. Most sulfides do not contain abundant Zn, limiting its use as internal standard to the analyses of sphalerite and wurtzite. In contrast, the most common sulfides pyrite, pyrrhotite, pentlandite, chalcopyrite and, to a lesser extent, sphalerite contain abundant Fe. The downside of the application of Fe as internal standard are the $^{40}Ar^{16}O$ interference on ^{56}Fe[25] and the availability of reference materials containing sufficient Fe. Many labs produce their own NiS fire assay buttons to apply as reference material which has generally low Fe concentrations[46, 47, 30]. Gilbert et al. (2013)[30] reported a Fe concentration of 350 µg g^{-1} in NiS3, significantly differing from Fe-sulfides and / or chalcopyrite and sphalerite. Nevertheless, there are sulfide reference materials available that contain abundant Fe (e.g. MASS-1, 15 %m/m[48]). The effect of the ArO interference on ^{56}Fe can be limited by either use of ^{57}Fe as the analyzed isotope or tuning of the mass spectrometer to low oxide production rates. Additionally, this interference would affect reference material and sample in the same way as long as Fe concentrations are in the same concentration range for both materials.

Most sulfides contain S in the concentration range of 30 to 55 %m/m, making S an ideal candidate for application as internal standard. Sylvester et al.(2001)[49] evaluated the interference of $^{16}O^{18}O$ on ^{34}S and found it to be ~1%, derived from air and equally affecting all sulfides. Wohlgemuth-Ueberwasser et al. (2007, 2014, 2015)[28, 50, 29] agree with these findings and did not observe any O interference on S relative to the high S concentrations of the samples, producing reasonable values for S and a variety of trace elements in different sulfide matrices and in cross analyses of different reference materials by tuning the mass spectrometer to oxide production rates of ThO/Th <0.5%. Nevertheless, Gilbert et al. (2013)[30] reported high and variable oxygen interferences on all S isotopes. They applied Ni as internal standard, deriving the Ni concentration in Fe-sulfide from LA-ICP-MS utilising an in-house borate glass reference material (STDGL2b-2[51]) which contains 441 µg g^{-1} Ni. Nickel concentration in Fe-sulfide was found to be 48 µg g^{-1} (<3% 2SD), significantly lower than Ni concentration in NiS3 (70.5 %m/m).

We analyzed Ni in Fe-sulfide from a similar batch (po = 8a; Gilbert et al.(2013)[30] used 8b[28]) applying NIST 610 as reference material and Fe as internal standard, as S in NIST 610 is too low. Utilisation of the 193 nm ns LA yielded a concentration of 110 ± 22 µg g^{-1}, the large variation probably related to the magnet that controls the ablation cup, influencing Ni as well as Fe as the internal standard in the aerosol.

Application of the 200 nm fs LA gave a Ni concentration of 103 ± 9 µg g^{-1}. With the 213 nm ns LA a Ni concentration of 87.7 ± 9 µg g^{-1} (10.3% 2SD) was obtained. Since the F.F. as well as the measurement accuracy determined as low deviation from reference values produced with the 213 nm ns LA show most reliable results, we used the Ni concentration yielded from this system for further calculations for all three LA systems. It should be noted that the uncertainty on the internal standard concentration does not propagate into the data processing using Iolite. Nickel was then applied as internal standard and NiS3 as reference material (NiS3(Ni)). The resulting concentrations for Rh, Pd, and Pt are given in table 2 and figure 1. Rhodium and Pt concentrations correspond to published values for 213 nm ns and 200 nm fs LA, but not for 193 nm ns LA. As Pd and Pt concentrations for 193 nm ns LA are also not matching published values this might again be attributed to the magnet regulating the ablation cup. Palladium does not accord to published values for all three LA systems. The use of S as internal standard produces generally more accurate and precise concentration data for Pd and Pt with 213 nm ns LA, and comparable measurement accuracy and precision with 200 nm fs LA, although it should be noted that precision is underestimated with NiS3(Ni) as the heterogeneity of the internal standard is neglected. This excess uncertainty would also apply for natural sulfides, where Ni is often heterogeneous distributed with up to 20% 2SD[29].

Role of the external standard in ns- and fs-LA-ICP-MS

To evaluate matrix effects we applied NIST 610 as reference material for PGE analyses in po with all three LA systems (table 2, figure 1). The 213 and 193 nm ns LA analyses yield too low concentrations that deviate from published values for Rh and Pt concentrations (figure 1 A, B, G, and H) and coincide for Pd concentration within uncertainty (figure 1 D and E). Concentrations derived from 200 nm fs LA are highly accurate and precise for Rh and Pt, but are significantly low for Pd (figure 1 C, F, and I). The higher precision achieved for Rh and Pt with NIST 610 as reference material can be attributed to the more homogeneous distribution of these elements in NIST 610 compared to NiS3. The deviation for Pd might be explained by the heterogeneity of Pd in NIST 610 with published values ranging from 0.96 to 1.41, with a value of 1.1 µg g^{-1} used within this study. A value closer to the upper reported concentration of 1.41 would shift the concentration upwards and match published values of po. Overall most accurate and precise concentrations for po could be obtained by 200 nm fs LA and application of NIST 610 as reference material. No matrix effects have been observed for fs LA.

Conclusions

1. No melting of any of the analyzed sulfides has been observed with application of fs LA in contrast to ns LA.

2. Most F.F. are around unity for all three LA systems. Elemental fractionation is not related to progressing ablation and deepening of the ablation crater.
3. Large uncertainties on F.F. can be assigned to the heterogeneous distribution of PGE in the corresponding sample and not to down-hole elemental fractionation.
4. Fe/S fractionation as evaluated by sensitivity of S and Fe in po and ccp is not observed from 213 nm ns LA, but from 193 nm ns LA and only S is affected in fs LA. As melting is highest with 213 nm ns LA, this fractionation cannot be attributed to melting.
5. Sulfur is an appropriate internal standard for ns LA-ICP-MS of sulfides as its concentration is in the same range for most sulfide specimen. Nevertheless, O interferences need to be avoided by tuning of the mass spectrometer to low oxide production rates. Due to the differences in S sensitivity among different minerals specimen with the 200 nm fs LA, Fe would be the recommended internal standard for this system.
6. Matrix effects in fs LA are negligible and Rh and Pt analyses show highest measurement accuracy and precision with application of NIST 610 as reference material. For the analysis of all PGE (including Os, Ru and Ir), sulfide reference materials are still necessary as to our knowledge no silicate reference material exists that contains Ru and / or Ir in concentrations above the detection limits usually reached by LA-ICP-MS and only one silicate reference material with Os (AGV[52]).

Acknowledgements

This study was supported with funds granted to C. C. W.-U. through Stockholm University. The PetroTectonics Analytical Facility was established with funding from the Knut and Alice Wallenberg Foundation. Marianne Ahlbohm is acknowledged for assistance in BSE-imaging and Ulrike Weiss for assistance in fs-LA-ICP-MS.

References

1 D. Günther and B. Hattendorf, *TrAC*, 2005, **24**, 255-265.

2 J. O'Reilly, D. Douglas, J. Braybrook, P.W. So, E. Vergucht, J. Garrevoet, B. Vekemans, L. Vincze and H. Goenaga-Infante, *J. Anal. At. Spectrom.*, **29,** 2014, pp. 1378–1384.

3 A. Taylor, M.P. Day, S. Hill, J. Marshall, M. Patriarca, M. White, *J. Anal. At. Spectrom.*, **29,** 2014, pp. 386–426.

4 M. Ohata, D. Tabersky, R. Glaus, J. Koch, B. Hattendorf, D. Günther, *J. Anal. Atom. Spectrom.* **19,** 2014, 1345 - 1353.

5 S. E. Gilbert, L. V. Danyushevsky, K. Goemann and D. Death, *J. Anal. Atom. Spectrom.*, 2014, **29**, 1024-1033.

6 D. Günther and J. Koch, *In Laser Ablation ICP–MS in the Earth Sciences: Current Practices and Outstanding Issues, Mineral. Assoc. of Canada, Quebec, Canada,* ed. P. Sylvester, 2008, 19-34.

7 D. Figg and M.S. Karr, *Appl. Spectrosc.*, **1997**, 511185-1192**,**

8 M.L. Alexander, M.R. Smith, J.S. Hatman, A. Mendoza and D.W. Koppenaal, *Appl. surf. sci.*, **1998**, 127-129, 255-261.

9 R.E. Russo, X.L. Mao, H.C. Liu, J.H. Yoo and S.S. Mao, *Appl. Phys. A Mater*., **1999,** 69, 887-894,

10 R. E. Russo, X. L. Mao, J. J. Gonzalez and S. S. Mao, *J. Anal. Atom. Spectrom.*, 2002, **17**, 1072-1075.

11 C. C. Garcia, H. Lindner, A. Von Bohlen, C. Vadla and K. Niemax, *J. Anal. Atom. Spectrom.*, 2008, **23**, 470-478.

12 L.V. Zhigilei, Z. Lin, and D.S. Ivano**v,** *J. Phys. Chem. C*, **2009,** *113*, 11892–11906.

13 S.S. Harilal, J.R. Freeman, P.K, Diwakar and A. Hassanein *In Laser-Induced Breakdown Spectroscopy, Springer Series in Optical Sciences*, (2014) 182, eds S. Musazzi and U. Perini, 143-166.

14 C. Cheng and X. Xu, *Phys. Rev. B*, 2005, **72**, 1-15.

15 P. Lorazo, L. Lewis and M. Meunier, *Phys. Rev. B*, 2006, **73**, 1-22.

16 H. Longerich, *In Laser Ablation ICP–MS in the Earth Sciences: Current Practices and Outstanding Issues, Mineral. Assoc. of Canada, Quebec, Canada,* ed. P. Sylvester, 2008, 1 – 18

17 S. E. Jackson, H. P. Longerich, G. R. Dunning and B. J. Fryer, *Can. Min.*, 1992**,** **30**, 1049-1064.

18 K. P. Jochum, B. Stoll, U. Weis, D. E. Jacob, R. Mertz-Kraus and M.O. Andreae, *Geostand. Geoanalyt. Res.*, 2014, **38**, 265-292.

19 M. Guillong, I. Horn and D. Günther, *J. Anal. Atom. Spectrom.*, 2003, **18**, 1224-1230.

20 J. Koch and D. Günther, *Anal. Bioanal. Chem.*, 2007, **387**, 149-153.

21 F. Poitrasson, X. Mao, S.S. Mao, R. Freydier and R. E. Russo, *Anal. Chem.*, 2003, **75**, 6184-6190.

22 I. Horn and F. von Blanckenburg, *Spectr. Acta B*, 2007, **62**, 410-422.

23 R. Glaus, R. Kaegi, F. Krumeich and D. Günther, *Spectrochim. Acta B*, 2010, **65**, 812-822.

24 P. K. Diwakar, S. S. Harilal, N. L. LaHaye, A. Hassanein and P. Kulkarni, *J. Anal. Atom. Spectrom.*, 2013, **28**, 1420-1429.

25 G. Velásquez, A. Y. Borisova, S. Salvi, and D. Béziat, *Geostand. Geoanalyt. Res.*, 2012, **36**, 315-324.

26 F.-X. D'Abzac, B. L. Beard, A. D. Czaja, H. Konishi, J. J. Schauer and C. M. Johnson, *Anal. Chem.*, 2013, **85**, 11885-11892.

27 F. Vanhaecke, M. Resano, J. Koch, K. McIntosh and D. Günther, *J. Anal. Atom. Spectrom.*, 2010, **25**, 1259-1267.

28 C. C. Wohlgemuth-Ueberwasser, C. Ballhaus, J. Berndt, V. Stotter nee Paliulionyte and T. Meisel, *Contr. Min. Petr.*, 2007, **154**, 607-617.

29 C. C. Wohlgemuth-Ueberwasser, F. Viljoen, S. Petersen and C. Vorster, *Geochim. Cosmochim. Acta*, 2015, **159**, 16-41.

30 S. Gilbert, L. Danyushevsky, P. Robinson, C. Wohlgemuth-Ueberwasser, N. Pearson, M. Norman, J. Hanley and D. Savard, *Geostand. Geoanalyt. Res.*, 2013, **37**, 51-64.

31 G. Kullerud, R. A. Yund and G. H. Moh, *In Magmatic Ore Deposits, Economic Geology Publishing Co., Lancaster, Pennsylvania*, ed. H. D. B. Wilson, 1969, 323-343.

32 G. Kullerud and R. A. Yund, *J. Petrol.*, 1962, **3**, 126-175.

33 M. E. Fleet, *Can. Min.*, 1988, **26**, 283-291.

34 L. J. Cabri and S. R. Hall, *Amer. Min.*, 1972, **57**, 689-708.

35 P. B. Barton, *Econ. Geol.*, 1973, **68**, 433-465.

36 P. J. Gardner and P. Pang, *J. Chem. Soc. Faraday Trans.*, 1988, **84**, 1879-1887.

37 J. Chmeleff, I. Horn, G. Steinhöfel and F. von Blanckenburg, *Chem. Geol.*, **2008**, 249, 155-166

38 J. Hellstrom, C. Paton, J. Woodhead and J. Hergt, *In Laser Ablation ICP–MS in the Earth Sciences: Current Practices and Outstanding Issues, Mineral. Assoc. of Canada, Quebec, Canada*, ed. P. Sylvester, 2008, 343-348.

39 C. Paton, J. C. Hellstrom, B. Paul, J. D. Woodhead and J. M. Hergt, *J. Anal. Atom. Spectrom.*, 2011, **26**, 2508-2518.

40 J. Woodhead, J. Hellstrom, J. Hergt, A. Greig and R. Maas, *Geostand. Geoanalyt. Res.*, 2007, **31**, 331-343.

41 B. J. Fryer, S. E. Jackson and H. P. Longerich, *Can. Min.*, 1995, **33**, 303-312.

42 A. J. Naldrett, *Magmatic Sulfide Deposits: Geology, Geochemistry and Exploration. Springer Verlag*, 2004, 728 p.

43 K. Pfaff, A. Koenig, T. Wenzel, I. Ridley, L. H. Hildebrandt, D. L. Leach and G. Markl, *Chem. Geol.*, 2011, **286**, 118-134.

44 P. J. Sylvester, *In Laser Ablation ICP–MS in the Earth Sciences: Current Practices and Outstanding Issues, Mineral. Assoc. of Canada, Quebec, Canada*, ed. P. Sylvester, 2008, 67–78.

45 D. A. Holwell, I. McDonald and I. B. Butler, *Contr. Min. Petr.*, 2011, **161**, 1011-1026.

46 R. W. Nesbitt, T. Hirata, I. B. Butler and J. A. Milton, *Geost. Newsl.*, 1997, **21**, 231-243.

47 E. K. Shibuya, J. E. S. Sarkis, J. Enzweiler, A. P. S. Jorge and A. M. G. Figueiredo A.M.G., *J. Anal. Atom. Spectrom.*, 1998, **13**, 941-944.

48 S. A. Wilson, W. I. Ridley and A. E. Koenig, *J. Anal. Atom. Spectrom.*, 2002, **17**, 406-409.

49 P. J. Sylvester, *In Laser Ablation ICP–MS in the Earth Sciences: Principles and Applications, Mineral. Assoc. of Canada, Quebec, Canada*, ed. P. Sylvester, 2001, 203-211.

50 C. C. Wohlgemuth-Ueberwasser, C. R. McClung and F. Viljoen, *Ore Geol. Rev.*, 2014, **56**, 45-52.

51 L. Danyushevsky, P. Robinson, S. Gilbert, M. Norman, R. Large, P. McGoldrick and M. Shelley, *Geochem. Explor. Env. A.*, 2011, **11**, 51-60.

52 S. A. Wilson, *The collection, preparation and testing of USGS reference material BCR-2, Columbia River Basalt.* U.S. Geological Survey Open-File Report, 1997.